OPEN

Virus activated artificial ECM induces the osteoblastic differentiation of mesenchymal stem cells without osteogenic supplements

Jianglin Wang, Lin Wang, Xin Li & Chuanbin Mao

Department of Chemistry and Biochemistry, Stephenson Life Sciences Research Center, University of Oklahoma, Norman, OK 73019, USA.

Biochemical and topographical features of an artificial extracellular matrix (aECM) can direct stem cell fate. However, it is difficult to vary only the biochemical cues without changing nanotopography to study their unique role. We took advantage of two unique features of M13 phage, a non-toxic nanofiber-like virus, to generate a virus-activated aECM with constant ordered ridge/groove nanotopography but displaying different fibronectin-derived peptides (RGD, its synergy site PHSRN, and a combination of RGD and PHSRN). One feature is the self-assembly of phage into a ridge/groove structure, another is the ease of genetically surface-displaying a peptide. We found that the unique ridge/groove nanotopography and the display of RGD and PHSRN could induce the osteoblastic differentiation of mesenchymal stem cells (MSCs) without any osteogenic supplements. The aECM formed through self-assembly and genetic engineering of phage can be used to understand the role of peptide cues in directing stem cell behavior while keeping nanotopography constant.

S tem cell niche as a specific extrinsic mircoenvironment integrate a complex array of molecular signals that, in combination with induced cell-intrinsic regulatory networks, control stem cell function and balance their numbers in response to physiological demands[1,2]. In most instances, stem cells in the niche are in contact with extracellular matrix (ECM), which provides multiple structural and biochemical cues to govern a series of stem cell behaviors in the temporal and spatial dimension[3,4]. Thus, more attention is being paid to the design of artificial ECM (aECM) by integrating some physical, chemical and/or mechanical factors into biomaterials for directing stem cell functions.

Nanotopography as a particular physical factor is now receiving more interest because it has advantageous features such as a large surface-to-volume ratio and a higher degree of biological plasticity compared with conventional micro- or macrostructures[5]. Emerging literature presents many interesting findings on how nanotopography enhances cell adhesion, alters cell morphology, affects cell expansion, initiates intracellular signaling, provides contact guidance and mediates stem cell differentiation[5–9]. Considering nanoscale topography in the design of biomimetic materials is a fashional idea because the resulting materials resemble the *in vivo* niche. On the other hand, biochemical cues as a traditional regulatory factor in the stem cell niche have been widely studied for a long time[10–12]. These signals can be classified into three types, including integral membrane proteins, localized secreted ECM components and soluble proteins like growth factors and cytokines[2]. The biochemical cues have been demonstrated to affect stem cell fates by targeting some specific signaling pathways such as β1 integrins activated MAPK signaling, Wnt signaling pathway in the hematopoietic stem cell (HSC) and Notch signaling in the development of the nervous system[13–15]. Therefore, it is increasingly interesting to introduce biochemical factors into artificial materials to directly control cell behaviors.

M13 filamentous phage, a virus that specifically infects bacteria and is harmless to human beings, is a bionofiber (∼880 nm long and ∼6.6 nm wide)[8,16]. It is made of DNA as a core and protein coat as a sheath that wraps the core. The coat protein constituting the side wall of phage is termed pVIII and encoded by gene VIII of the phage DNA. Compared to other nanofibers, M13 phage is unique in that it can not only be used as an organic building block to build 2-D films and 3-D scaffolds with unique topographical structures through self-assembly, but also introduce different peptides on the constituent building block to provide biochemical cues by the

well-established phage display technique[7,8]. Inserting a foreign gene into gene VIII leads to the display of a foreign peptide as fusion to pVIII and the concomitant presentation of foreign peptide on the side wall of phage. The ease of displaying a peptide on the side wall of phage nanofibers enables us to use phage to study the peptide cues (biochemical cues) that can direct the stem cell fate. In addition, the ease of assembly of phage nanofibers into a nanostructured film further gives us the capability of studying the stem cell fate on a nanostructure with specific peptide sequence displayed on the phage nanofibers that generate a unique nanotopography. These unique properties of phage allow us to systematically study the effect of different peptides on the substrates with constant nanotopography on the stem cell fate (**Figure 1**).

In this communication, we employed a phage display approach to generate a virus-activated aECM with well-defined topographical and biochemical cues to activate the regulation of the morphology, proliferation and osteoblastic differentiation of rat mesenchymal stem cells (MSCs). We separately displayed different fibronectin-derived peptides (RGD, its synergy site PHSRN, and a combination of RGD and PHSRN) on the side wall of phage nanofibers through phage display technique, and assembled them into a 2-D film based on our established layer-by-layer self-assembly method[8]. We chose to study the two fibronectin-derived peptides to be displayed on phage surface based on the following considerations. Fibronectin is a crucial ECM component of many tissues and regulates a variety of cell activities predominantly through direct interactions with cell surface integrin receptors[17]. The identified adhesive domains of the

fibronectin are comprised of at least two minimal and pivotal peptide sequences, including an Arg-Gly-Asp (RGD) sequence located in the 10th type III repeating unit and a Pro-His-Ser-Arg-Asn (PHSRN) sequence in the 9th type III repeating unit[18]. The RGD and PHSRN sequences as pervasive adhesive peptides can influence multiple cell behaviors including cell adhesion, proliferation and differentiation[17,19–22].

Results

Self-assembly of phage-based films. Due to the long-rod structure and monodispersity of phage nanofibers[7,23], they were firstly assembled into bundles, which were further assembled in a parallel format to form a 2-D phage-based film material on poly-L-lysine substrate (Figure 1B). The resultant film showed a slightly rough surface and ordered ridge/groove topography (**Figure 2**). The formation of the phage-based film was driven through liquid crystalline phase transitions at the air-liquid interface during the evaporation process[6,8,24]. In addition, the electrostatic interaction between negatively chargely phage nanofibers and positively chargely polylysine substrate provided another driving force to promote the assembly of phage bundles into films with a unique highly ordered topography where phage bundles as ridges were parallel to each other and separated by grooves.

Morphology and nanotopography of phage-based films. We found that the specific ordered ridge/groove topography was controlled by the concentration of phage solution during layer-by-layer assembly.
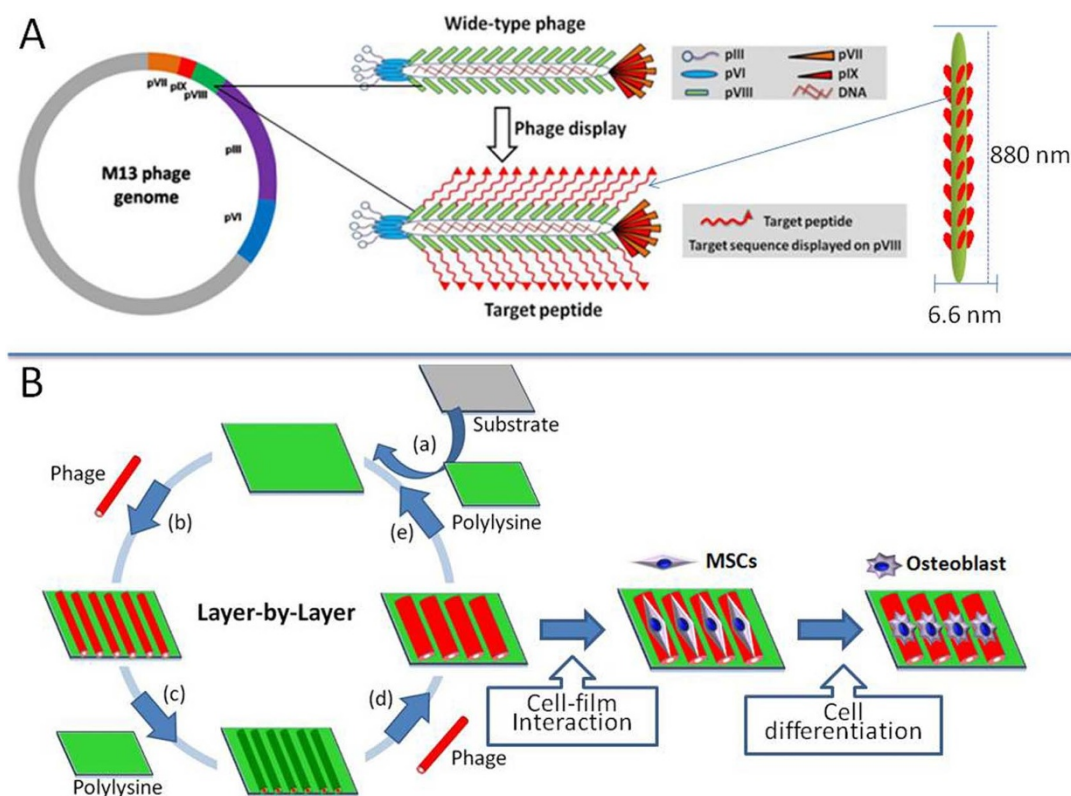
Figure 1 | Schematic diagram of using phage display technique to produce biomaterials with both unique nanostructures derived from a layer-by-layer method and functional peptides displayed for directing stem cell fate. Foreign peptides (RGD or PHSRN) derived from fibronectin were separately inserted and displayed in the N-terminal end of major coat protein (pVIII) constituting the side wall of M13 phage (1A). The phage bundles were generated based on the unique properties of long-rod structure and monodispersity of phage nanofibers in the desired phage concentration, and the engineered phage bundles were further used to form phage-based film biomaterials via a layer-by-layer self-assembly method (1B). The polylysine was introduced as the first positively charged layer on the substrate, and then the engineered phage, which was anionic due to the presence of anionic amino acid residues in the major coat protein, was deposited as a second negatively charged layer. This process was repeated for three times and a phage-based film was formed with phage as a terminating layer (1B, a-e). The resultant phage-based films with precisely introduced peptide sequences (surface chemistry) and well-defined ridge/groove topographical feature were found to direct osteoblastic differentiation of mesenchymal stem cells (MSCs).
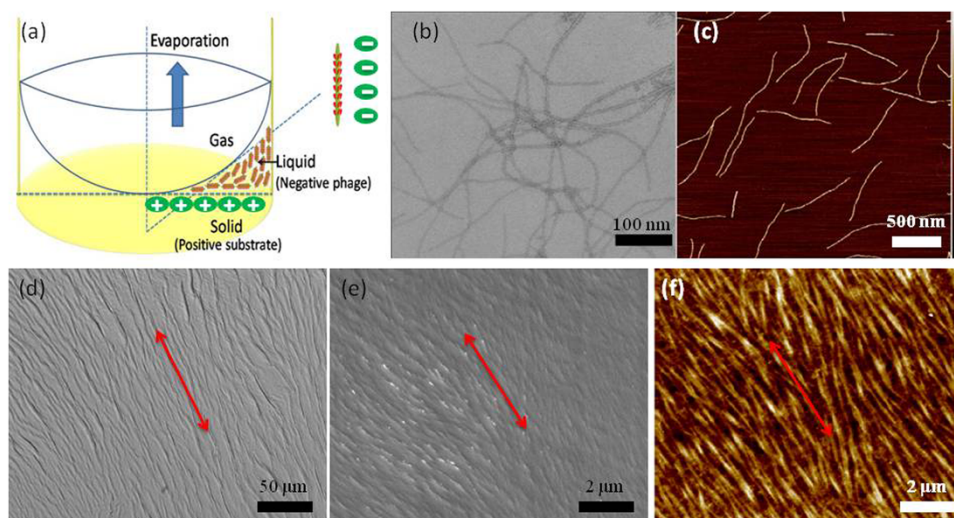
Figure 2 | Preparation and characterization of phage-based film materials. The M13 phage with nanofiber-like structure and monodispersity was driven to form a film by liquid crystalline phase transitions at the arc-shaped air-liquid interface and electrostatic interaction between negatively charged phage nanofibers and positively charged polylysine substrate (a). The morphology and size of individual phage nanofibers before they were used to form a film were observed by TEM and AFM (b and c). The phage nanofibers were further assembled to form a phage-based film with a unique topography of ridge/groove nanostructure (d, bright field; e, SEM; f, AFM; the red arrows highlight the highly oriented self-assemblies of phage bundles).

The diameter of phage bundles was around 1000 nm at the higher phage concentration (10^{14} pfu/ml) whereas the diameter was about 500 nm at the lower phage concentration (10^{12} pfu/ml) (**Figure 3**). In addition, our current data showed that the roughness of phage-based films was dependent on the phage concentration and increased with the rise of the phage concentrations (**Figure 4**). Therefore, the surface topography of phage films could be regulated by altering the size of phage bundles, which could be controlled by varying the phage concentrations.

Cell adhesion on the phage-based films. The rat MSCs were used to evaluate the biological functions of the unique biofilm materials. Our current data confirmed that the ordered ridge/groove structure represented by the phage films significantly induced the elongation

and parallel alignment of MSCs along phage bundles in phage-based film materials for all of the peptide sequences displayed on the constituent phage nanofibers (**Figures 5a,5c & 5e**). However, cell elongation and alignment were not detected on the phage film derived from higher concentration of phage solution of 10^{14} pfu/ml (**Figures 5b,5d & 5f**) and the control substrate (i.e., polylysine substrate without phage material) (**Supplementary Figure S1**). The significant cell elongation and alignment was also missing if the phage concentration was lower than 10^{12} pfu/ml. Therefore, the optimal concentration of phage solution was defined between 10^{12} pfu/ml and 10^{14} pfu/ml to form the suitable films, which were used to significantly stimulate cell elongation. As shown in **Figure 3d**,
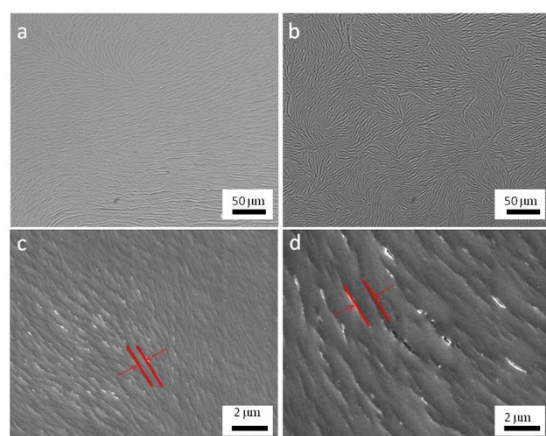
Figure 3 | Morphology of phage-based film derived from the different phage concentrations. The phage bundles derived from the lower concentration (10^{12} pfu/ml, a and c) of phage solution was smaller than those from the higher concentration of phage solution (10^{14} pfu/ml, b and d). The orientation of phage bundles between neighboring domains is similar and the phage nanofibers showed a longer range parallel alignment with each other in the lower concentration (a and c). However, the orientation of phage bundles was similar inside a small domain but different between neighboring domains in the high concentration (b and d).
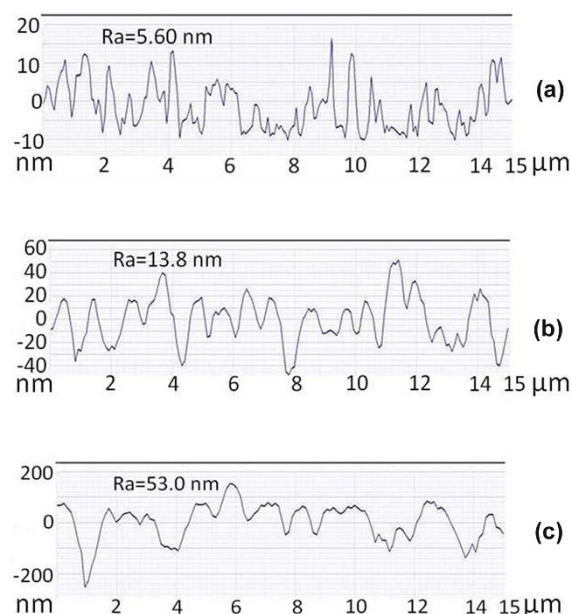
Figure 4 | The average surface roughness (Ra) of phage-based films derived from the different phage concentrations. The AFM surface line scan profile indicated that the surface roughness of phage films was increased with the rise of phage concentration (a, b and c denoted the phage concentration of 10^{12}, 10^{13} and 10^{14} pfu/ml, respectively).
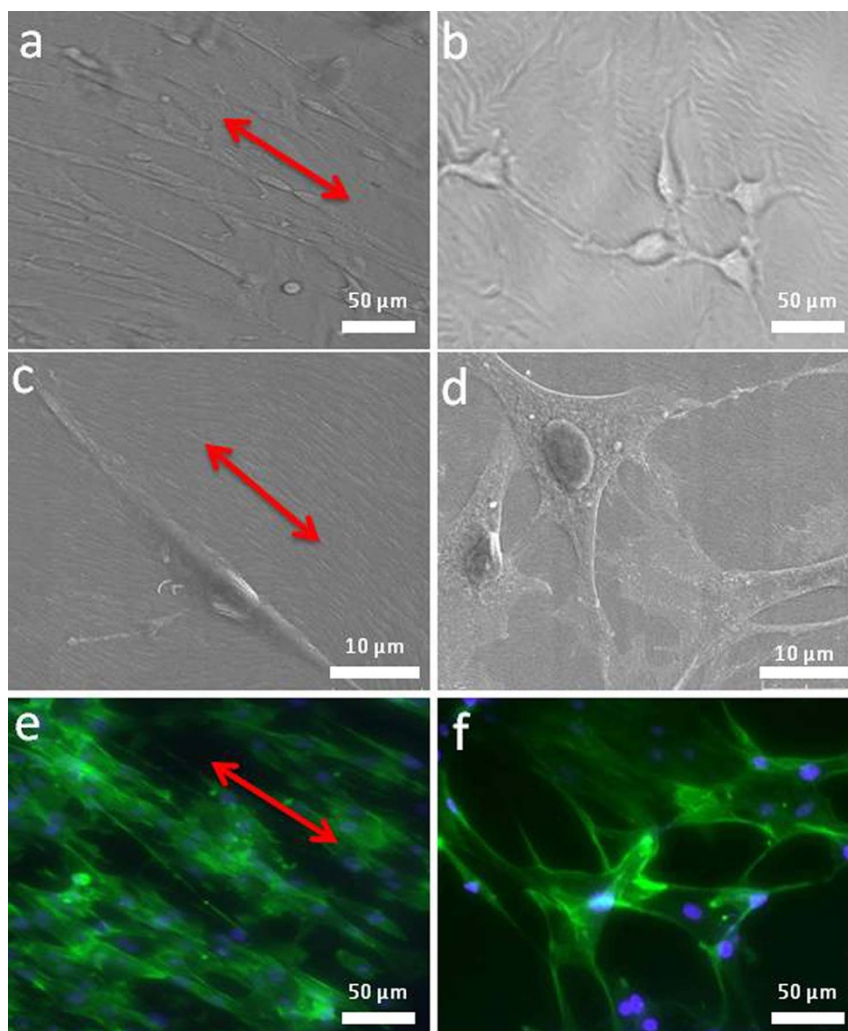
Figure 5 | Cell adhesion on the phage-based film derived from both low (a, c, e) and high (b, d, f) phage concentration. The MSCs on the phage-based film derived from the low phage concentration (10^{12} pfu/ml) were significantly elongated and aligned along phage bundles (a, c, e) whereas those on the phage-based film derived from the high phage concentration (10^{14} pfu/ml) were randomly oriented and not elongated (b, d, f). Images shown were taken from bright field optical microscopy (a, b), SEM (c, d) and fluorescence microscopy (e, f). Cell nuclei were stained by DAPI (blue) and F-actin were stained by FITC-labeled phalloidin (green).

on the films assembled from phage at a higher concentration, phage bundles are nearly aligned inside a domain with a size (20–25 µm) comparable to MSCs, however, the orientation of phage bundles between neighboring domains is different. Namely, the direction of elongation of phage bundles in different domains is different and the parallel alignment of nanofibers is only confined in a domain with size similar to MSCs. As a result, the MSCs growing on the films assembled from a higher concentration of phage are not oriented and aligned. Moreover, in the absence of phage bundles, the cells were completely randomly oriented due to the lack of contact guidance by the phage bundles. Therefore, the morphological changes and parallel alignments of MSCs on the phage-based film materials were mainly stimulated by the unique ordered ridge/groove surface topography but not by the peptide sequences displayed on the surface.

Cell proliferation and differentiation on the phage-based films. We proceeded to investigate cell proliferation on the films derived from phage nanofibers with different concentrations and peptides displayed. MTT results demonstrated that cell proliferation was influenced by both the peptide sequences displayed on the constituent phage nanofibers and the concentrations of the phage

solution (**Figures 6a & 6b**). Since the phage concentration influenced the size and separation of phage bundles to modulate the nanotopographical cues and the peptide sequences displayed on phage represented the biochemical cues, this fact implied that the cell proliferation was controlled by both topographical and biochemical cues.

To investigate the osteoblastic differentiation of MSCs on the phage-based film materials, the cell-materials were cultured in both primary and osteogenic differentiation media for 2 weeks. Immunofluorescence staining as a qualitative analysis at the protein level was used to verify the differentiation status. We found that osteocalcin (OCN) and osteopontin (OPN), the two osteogenesis-specific markers, presented positive staining on all materials in the primary media (**Figure 6d**). The OCN and OPN exbihited a higher expression on all phage-based materials than that on the control (poly-L-lysine substrate without phage film). Collagen I (COL) as a positive control of non-osteogenic marker showed high expression on all materials, and there was no significant difference between phage-based and control groups. Also, OCN and OPN presented positive staining in all materials and their expression was significantly enhanced in the osteogenic differentiation media (**Supplementary Figure S2**) as compared to in the primary media. Real-time polymerase
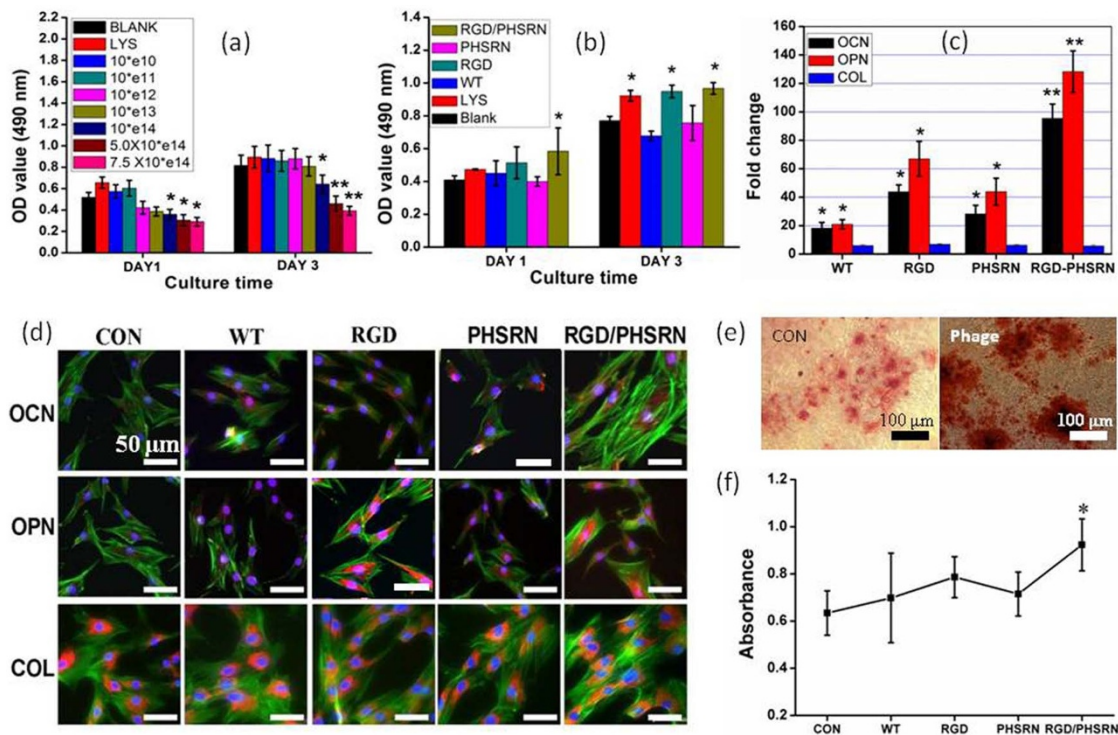
Figure 6 | Cell proliferation and differentiation on the phage-based materials in the primary media. Cell proliferation was significantly influenced by phage concentration and phage types (a, b). Cell differentiation was regulated by different peptides displayed on the engineered phage types (c, d). The ALP activity assay (f) and alizarin red staining (e) further demonstrated that the osteoblastic differentiation of MSCs was induced by phage-based film materials. All data represented the mean ± standard deviation (n = 3, * p<0.05, **p<0.01). WT, RGD, PHSRN and RGD/PHSRN denoted films made of wild type phage, RGD-displayed phage, PHSRN-displayed phage, and a mixture of RGD- and PHSRN-displayed phage, respectively. CON and LYS denoted poly-L-lysine substrates without phage. BLANK denoted pure glass substrate. OCN, OPN and COL were stained by rhodamine-labeled antibody (red) and cell nuclei were stained by DAPI (blue) and F-actin were stained by FITC-labeled phalloidin (green).

chain reaction (PCR) assay was used to further analyze the relative gene level of the osteogenic markers associated with MSCs differentiation on the phage-based materials in the primary media (**Figure 6c**). Both OCN and OPN genes were found to show significant up regulation on the phage-based film materials compared to the control group. Among the different engineered phage nanofibers, RGD/PHSRN-phage presented an extremely high mRNA level of the two osteogenesis-specific proteins (OCN and OPN) in comparison to the control group (**, $p < 0.01$). RGD-phage, PHSRN-phage and WT-phage showed higher expression of OCN and OPN genes than the control (*, $p < 0.05$). However, COL gene as a non-specific osteogenic marker did not show significant difference between phage-based materials and the control. The phage-based groups still showed significant up-regulation of mRNA level for both OCN and OPN genes under the condition of osteogenic media (**Supplementary Figure S3**). Overall, the phage-based materials enabled to induce the osteoblastic differentiation of MSCs in the primary media without any osteogenic supplements, and the osteoblastic differentiation was further enhanced in the presence of both materials and osteogenic differentiation media.

ALP as a marker protein specific for the osteoprogenitor activity was normally used to verify the osteoblastic differentiation of MSCs. The ALP assay demonstrated that both phage-based material and control groups showed positive ALP expression (**Figure 6f**). However, the group of RGD/PHSRN-phage presented the highest ALP activity among all groups. The typical alizarin red staining was used to confirm the osteogenic mineralization by detecting the formation of calcium nodule (**Figure 6e**). The positive staining of calcium nodule was detected on all materials. Furthermore, the staining on the phage-based film materials was much stronger than that in the control. These results suggest the RGD/PHSRN-phage with

unique nanotopography promoted the osteoblastic differentiation of MSCs, suggesting a synergetic enhancement by both the biochemical and topographical cues.

Discussion

Compared to other nanofibers, M13 phage is unique because it can not only be used as a building block to build unique ridge/groove structures through self-assembly, but also introduce different peptides on the constituent building block into the resultant ridge/groove structures by the well-established phage display technique[7,8]. This unique property of phage enables us to systematically study the effect of different peptides on the substrates with constant topography on the stem cell fate. In this study, we constructed different recombinant engineered phages to display adhesive signaling peptide of RGD and PHSRN derived from fibronectin, respectively. Both RGD and PHSRN motifs have been identified as pervasive adhesive peptides to mediate multiple cell activities including cell adhesion, proliferation and differentiation[17,19–22], and have been widely used to design the smart biomaterials. Traditionally, such peptides are physically mixed into or chemically immobilized onto biomaterials, preventing us from forming aECM with ordered assembly of peptides and varying only the peptide sequences without changing topography in studying stem cell fates. Therefore, phage display is a unique approach to studying stem cell fate because it allows us to precisely introduce foreign peptide into a nanotopography by genetic means and the nanotopography can be generated by its self-assembly behavior. In addition, the fact that the self-assembly of phage is not affected by the peptide displayed on its surface makes it possible to form an ECM with different peptides but a constant nanotopography for us to systematically study the effect of peptide cues on the stem cell behavior.

M13 phage as a natural nanofiber (∼880 nm by 6.6 nm) can be assembled into bundles due to its long-rod structure and monodispersity[7,23]. The phage bundles can be further aligned to form phage-based 2-D film materials through two driving forces. One is the liquid crystalline assembly at the air-liquid interface during the evaporation process[6,8,24], another is the electrostatic interaction between negatively chargely phage nanofibers and positively chargely polylysine. As a result, an ECM was produced with a unique highly ordered topography where phage bundles as ridges are parallel to each other and separated by grooves (**Figure 2**). In addition, tuning the concentration of the phage suspension used for self-assembly on the substrate can control the size and surface roughness of phage bundles constituting the film (**Figures 3 and 4**).

It has been reported that the topography of culture substrate influences the cell behaviors by elongating cell shape[5,25–27]. Dalby et al demonstrated that the topographical cue based on the use of disordered nanopits in the polymethylmethacrylate (PMMA) substrate can stimulate the osteoblastic differentiation of human MSCs without the osteogenic supplements[28]. The mechanism might be that the disordered nanopits resulted in longer adhesion, which impacts cytoskeleton tension. These changes in adhesion and cytoskeleton tension will have an effect on cell behavior through an indirect mechanotransductive pathway. Moreover, Jin et al showed that the topographical cue generated from the nanotubular-shaped titanium oxide regulated the osteogenic differentiation of hMSCs[5]. The possible mechanism is that topography-induced cell elongation stimulates the stem cell differentiation. Our current data also confirm that the ordered ridge/groove structure represented by the phage films significantly induced the elongation and parallel alignment of MSCs along phage bundles in phage-based film materials for all of the peptide sequences displayed on the constituent phage nanofibers. Therefore, the morphological changes of MSCs on phage-based film materials might further stimulate the mechanical difference of cytoskeleton, which plays a pivotal role in regulating mechanotransductive pathways and finally having an impact on multiple stem cell behaviors[26]. Although different topographical cues including nanopits[28], nano-tube[5] or nano-bundle (our work) are designed on the different substrates, including polymer (PMMA[28]), metal (TiO$_2$[5]) and biomolecule (phage), respectively, to stimulate stem cell behavior, the nature of regulatory mechanism might be similar. That is, cell shape is changed by modulating cell adhesion on the substrate materials and finally stem cell fate is directed by biomechanical difference or mechanotransductive pathway.

The MTT result demonstrates that cell proliferation is influenced by both the peptide sequences displayed on the constituent phage nanofibers and the concentrations of the phage nanofibers (**Figures 6a & 6b**). Since the phage concentration influences the size and separation of phage bundles to modulate the nanotopographical cues and the peptide sequences displayed on phage represents the biochemical cues, we can conclude that stem cell morphology and alignment are solely modulated by the topographical cue, whereas the cell proliferation is directed by both topographical and biochemical cues.

In order to further understand the effect of both topographical and biochemical cues on cell differentiation, we design two culture systems including primary and osteogenic media to elucidate which factors influence stem cell differentiation. It is widely demonstrated that the osteogenic differentiation media as a chemical stimulation plays a key role in enhancing osteoblastic differentiation of multiple stem cells including embryonic stem cells, induced pluripotent stem cells and adult stem cells[29–31]. Our current results also support that conclusion. Moreover, we simultaneously confirm that the successful induction of osteoblastic differentiation can be performed in the media without any osteogenic supplements (**Figures 6c & 6d**). This fact means that the material itself can direct the osteoblastic differentiation of MSCs through its topographical and biochemical

features in the absence of osteogenic supplements. However, the osteogenic differentiation of MSCs is extremely enhanced when the MSCs are cultured on the materials in concert with osteogenic media (**Figures S2 & S3**).

RGD and PHSRN motifs derived from fibronectin, which is a major adhesive component in the natural ECM, have been widely demonstrated to mediate the stem cell behaviors through specific integrin signal pathway[32]. The osteoprogenitor cells expressed some integrins, including $\alpha_5\beta_1$ specifically binding with RGD and RGD-PHSRN, to regulate osteoblast survival, proliferation, osteogenic gene expression and matrix mineralization[17,21]. Our results showed that a combination of RGD and PHSRN presented on a unique ridge/groove nanotopography significantly enhanced osteoblastic differentiation (**Figures 4b & 4c**). Therefore, the osteoblastic differentiation of MSCs on the phage-based film were significantly stimulated by both topographical and biochemical cues.

In conclusion, designing materials to direct stem cell fate has a profound impact on stem cell biology and provides insights that will facilitate the clinical application of stem cells in modern regenerative medicine. In this study, a virus-activated aECM with controlled biochemical and topographical cues was precisely designed to mediate stem cell behavior. This specific aECM is characteristic of highly ordered topography with aligned ridge/groove nanostructures, which result from the self-assembly of phage nanofibers, and simultaneously presents the biochemical signals made of RGD and PHSRN peptides by phage display technique. The current data demonstrate that cell alignment and elongation are mainly regulated by topographical cues. Cell proliferation are greatly influenced via a combination of topographical and biochemcial cues. Due to the presence of the unique ridge/groove nanostructure made of phage nanofibers and the fibronectin derived peptides displayed on the phage nanofibers, the aECM can stimulate the osteoblastic differentiation of MSCs in the primary media without osteogenic supplements. The same aECM can further enhance the osteogenic differentiation of MSCs once in osteogenic media. Our findings suggest that a proper combination of unique nanotopographical and biochemical cues can control the stem cell behaviors including induction of the osteoblastic differentiation. Our phage display approach represents a novel strategy for generating a virus-activated aECM, where peptide sequences can be systematically tuned on a unique, constant nanotopography by genetic means, for probing the biochemical cues in directing stem cell fate.

Methods

Peptides display and films fabrication. RGD and PHSRN were respectively displayed on the N-terminus of pVIII, which was the major coat protein constituting the external side wall of M13 bacteriophage, by following our reported protocols (**Figure 1A**)[33–35]. Filamentous phages were assembled into films following a layer-by-layer self-assembly method developed by our group (**Figure 1B**)[8]. Briefly, the disc-shaped cover slide was sonicated and washed with DI water, and placed into each well of 24-well culture plate. The poly-L-lysine solution (0.01%) was added to the well with cover slide to form the first layer with positive charge on the cover slide. After drying, the phage solution was added to form the secondary layer with negative charge. The process was repeated for three times and a film was formed on the cover slide with phage as a terminating layer. The morphologies of the individual phage nanofibers were observed by transmission electron microscope (TEM, ZEISS 10A) and Atomic force microscope (AFM, BioScope Catalyst, Bruker) and the fabricated films were examined by optical microscope, fluorescence microscope and scanning electron microscope (SEM, JSM-840A).

Cell culture and seeding. Rat MSCs were purchased from Invitrogen (No: S1601-100) and expanded in the primary media, which contained Dulbecco's Modified Eagle Media (DMEM, Gibco), 15% fetal bovine serum (FBS, Gibco) and 1% antibiotics (penicillin 100 U/ml, streptomycin 100 U/ml). The MSCs in their third passage were seeded onto the phage-based films, and then cultured separately in primary and osteogenic differentiation media (Thermo scientific, Advance STEMO steogenic Differentiation Kit). The media was replaced twice a week and the culture was terminated after two weeks.

Cell proliferation. For study of cell viability and proliferation, the MSCs were seeded onto the phage-based film materials to investigate the biocompatibility of different

materials and the effects of different concentrations of phage used to make the films in the primary media. The phage concentration was varied from low to high values, including 10^{10} pfu/ml, 10^{11} pfu/ml, 10^{12} pfu/ml, 10^{13} pfu/ml, 10^{14} pfu/ml, 5.0×10^{14} pfu/ml and 7.5×10^{14} pfu/ml. The cell proliferation was then measured by 3-(4,5-dimethylthiazol-2-yl)-2,5-diphenyl tetrazolium bromide (MTT, Sigma) staining at the designed time points including day 1 and day 3. The cell-film complex was incubated in the MTT solution (20 μl, 5 mg/ml) at 37°C in 5% CO_2 incubator for 4 h. The intense purple formazan derivative formed via cell metabolism was eluted and dissolved in 150 μl/well dimethylsulfoxide (DMSO, Sigma). The absorbance was measured at 490 nm on a plate reader (Biotek, USA).

Immunofluorescence staining. All engineered phage films for osteoblastic differentiation were derived from the constant phage concentration of 10^{13} pfu/ml. After cultured for 2 weeks in primary and osteogenic differentiation media, the cells on the films were washed and fixed with 4% paraformaldehyde at 4°C for 30 min. They were permeablized using 0.3% Triton X-100 for 5 min and then blocked with 5% goat serum solution for 1 h at room temperature. After blocking, the cells were incubated overnight at 4°C with the primary antibodies targeting the osteo-specific proteins (Osteocalcin, OCN and osteopontin, OPN) and non-osteo-specific protein (collagen I-α1, COL). Secondary antibody labeled by TRITC was used for labeling OCN, OPN, and COL, respectively, at 1:1000 dilutions in a blocking buffer for 1 h at room temperature. Alexa Fluor 488 phallodin (1:400 in PBS) and DAPI (4,6-diamidino-2-phenylindole) were used to stain the actin filaments and nuclei, respectively. Images of the stained samples were collected with a fluorescence microscope (Nikon, Ti-S).

Real-time polymerase chain reaction (PCR). Real-time PCR was further assayed by Ambion Power SYBR Green cells-to-Ct Kit (Invitrogen, US) in both primary and osteogenic differentiation media. The template cDNA was amplified with real-time quantitative PCR using gene-specific primers of OCN, OPN and COL. Acidic ribosomal phosphoprotein (Arbp) was used as a reference gene. Sequences of the primers in this study were shown in **Table S1**. The real-time PCR reaction was done using the following protocol: initial denaturation at 95°C for 5 min and 45 cycles of PCR (95°C for 30 s, 58°C for 30 s and 72°C for 45 s). The assay was carried out in triplicate and relative gene expression was calculated with respect to the gene expression in the control substrate without phage film[36].

Assays of alkaline phosphatase and mineralization of the cell-matrix. After culture for two weeks in the primary media, the MSCs seeded on phage-based film materials were tested for alkaline phosphatase (ALP) activity and calcium nodule staining. The ALP activity was performed by p-nitrophenyl phosphate (pNPP) method. Briefly, the pNPP was used as a substrate for ALP to be hydrolysed to form a soluble yellow reaction products at pH 10.5 and 37°C. The staining reaction was terminated by the addition of 3 M NaOH and the final color showed a maximum absorbance at 405 nm. For calcium nodule staining, the cells were fixed in 4% paraformaldehyde at 4°C for 15 min and then stained with 0.2% alizarin red at pH 5.0 for 15 min. The staining images were collected with optical microscope.

Statistical analyses. All experimental analysis of cell proliferation, real-time PCR and ALP assay were performed in triplicate (n = 3). The data were expressed as mean ± SD (standard deviation) at a significance level of $p < 0.05$. Differences among groups were determined by a one-way ANOVA with a Bonferroni *post hoc* analysis with SPSS software (version. 17).

1. Morrison, S. J. & Spradling, A. C. Stem cells and niches: Mechanisms that promote stem cell maintenance throughout life. *Cell* **132**, 598–611 (2008).
2. Lutolf, M. P. & Blau, H. M. Artificial Stem Cell Niches. *Advanced Materials* **21**, 3255–3268 (2009).
3. Watt, F. M. & Hogan, B. L. M. Out of Eden: Stem cells and their niches. *Science* **287**, 1427–1430 (2000).
4. Even-Ram, S., Artym, V. & Yamada, K. M. Matrix control of stem cell fate. *Cell* **126**, 645–647 (2006).
5. Oh, S. *et al*. Stem cell fate dictated solely by altered nanotube dimension. *Proceedings of the National Academy of Sciences of the United States of America* **106**, 2130–2135 (2009).
6. Chung, W.-J. *et al*. Biomimetic self-templating supramolecular structures. *Nature* **478**, 364–368 (2011).
7. Merzlyak, A., Indrakanti, S. & Lee, S.-W. Genetically Engineered Nanofiber-Like Viruses For Tissue Regenerating Materials. *Nano Letters* **9**, 846–852 (2009).
8. Zhu, H. *et al*. Controlled growth and differentiation of MSCs on grooved films assembled from monodisperse biological nanofibers with genetically tunable surface chemistries. *Biomaterials* **32**, 4744–4752 (2011).
9. Kilian, K. A., Bugarija, B., Lahn, B. T. & Mrksich, M. Geometric cues for directing the differentiation of mesenchymal stem cells. *Proceedings of the National Academy of Sciences of the United States of America* **107**, 4872–4877 (2010).
10. Discher, D. E., Mooney, D. J. & Zandstra, P. W. Growth Factors, Matrices, and Forces Combine and Control Stem Cells. *Science* **324**, 1673–1677 (2009).
11. Kubota, H., Avarbock, M. R. & Brinster, R. L. Growth factors essential for self-renewal and expansion of mouse spermatogonial stem cells. *Proceedings of the National Academy of Sciences of the United States of America* **101**, 16489–16494 (2004).
12. Yamashita, Y. M., Fuller, M. T. & Jones, D. L. Signaling in stem cell niches: lessons from the Drosophila germline. *J. Cell Sci.* **118**, 665–672 (2005).
13. Zhu, A. J., Haase, I. & Watt, F. M. Signaling via beta 1 integrins and mitogen-activated protein kinase determines human epidermal stem cell fate in vitro. *Proceedings of the National Academy of Sciences of the United States of America* **96**, 6728–6733 (1999).
14. Duncan, A. W. *et al*. Integration of Notch and Wnt signaling in hematopoietic stem cell maintenance. *Nature Immunology* **6**, 314–322 (2005).
15. Artavanis-Tsakonas, S., Rand, M. D. & Lake, R. J. Notch signaling: Cell fate control and signal integration in development. *Science* **284**, 770–776 (1999).
16. Mao, C., Liu, A. & Cao, B. Virus-Based Chemical and Biological Sensing. *Angewandte Chemie-International Edition* **48**, 6790–6810 (2009).
17. Martino, M. M. *et al*. Controlling integrin specificity and stem cell differentiation in 2D and 3D environments through regulation of fibronectin domain stability. *Biomaterials* **30**, 1089–1097 (2009).
18. Hynes, R. O. INTEGRINS - VERSATILITY, MODULATION, AND SIGNALING IN CELL-ADHESION. *Cell* **69**, 11–25 (1992).
19. Jeschke, B. *et al*. RGD-peptides for tissue engineering of articular cartilage. *Biomaterials* **23**, 3455–3463 (2002).
20. Hersel, U., Dahmen, C. & Kessler, H. RGD modified polymers: biomaterials for stimulated cell adhesion and beyond. *Biomaterials* **24**, 4385–4415 (2003).
21. Garcia, A. J. & Reyes, C. D. Bio-adhesive surfaces to promote osteoblast differentiation and bone formation. *Journal of Dental Research* **84**, 407–413 (2005).
22. Tosatti, S. *et al*. RGD-containing peptide GCRGYGRGDSPG reduces enhancement of osteoblast differentiation by poly(L-lysine)-graft-poly(ethylene glycol)-coated titanium surfaces. *Journal of Biomedical Materials Research Part A* **68A**, 458–472 (2004).
23. Chiang, C.-Y. *et al*. Weaving genetically engineered functionality into mechanically robust virus fibers. *Advanced Materials* **19**, 826–+ (2007).
24. Lin, Y., Balizan, E., Lee, L. A., Niu, Z. & Wang, Q. Self-Assembly of Rodlike Bio-nanoparticles in Capillary Tubes. *Angewandte Chemie-International Edition* **49**, 868–872 (2010).
25. Biggs, M. J. P. *et al*. Interactions with nanoscale topography: Adhesion quantification and signal transduction in cells of osteogenic and multipotent lineage. *Journal of Biomedical Materials Research Part A* **91A**, 195–208 (2009).
26. Biggs, M. J. P. *et al*. Adhesion formation of primary human osteoblasts and the functional response of mesenchymal stem cells to 330 nm deep microgrooves. *Journal of the Royal Society Interface* **5**, 1231–1242 (2008).
27. Engler, A. J., Sen, S., Sweeney, H. L. & Discher, D. E. Matrix elasticity directs stem cell lineage specification. *Cell* **126**, 677–689 (2006).
28. Dalby, M. J. *et al*. The control of human mesenchymal cell differentiation using nanoscale symmetry and disorder. *Nature Materials* **6**, 997–1003 (2007).
29. Buttery, L. D. K. *et al*. Differentiation of osteoblasts and in vitro bone formation from murine embryonic stem cells. *Tissue Engineering* **7**, 89–99 (2001).
30. Bilousova, G. *et al*. Osteoblasts Derived from Induced Pluripotent Stem Cells Form Calcified Structures in Scaffolds Both in Vitro and in Vivo. *Stem Cells* **29**, 206–216 (2011).
31. Schneider, R. K. *et al*. The osteogenic differentiation of adult bone marrow and perinatal umbilical mesenchymal stem cells and matrix remodelling in three-dimensional collagen scaffolds. *Biomaterials* **31**, 467–480 (2010).
32. Keselowsky, B. G., Collard, D. M. & Garcia, A. J. Integrin binding specificity regulates biomaterial surface chemistry effects on cell differentiation. *Proceedings of the National Academy of Sciences of the United States of America* **102**, 5953–5957 (2005).
33. Liu, A., Abbineni, G. & Mao, C. Nanocomposite Films Assembled from Genetically Engineered Filamentous Viruses and Gold Nanoparticles: Nanoarchitecture- and Humidity-Tunable Surface Plasmon Resonance Spectra. *Advanced Materials* **21**, 1001–1005 (2009).
34. Xu, H., Cao, B., George, A. & Mao, C. Self-Assembly and Mineralization of Genetically Modifiable Biological Nanofibers Driven by beta-Structure Formation. *Biomacromolecules* **12**, 2193–2199 (2011).
35. Mao, C. B., Wang, F. & Cao, B. Controlling nanostructures of mesoporous silica fibers by supramolecular assembly of genetically modifiable bacteriophage. *Angewandte Chemie International Edition* **51**, 6411–6415 (2012).
36. Livak, K. J. & Schmittgen, T. D. Analysis of relative gene expression data using real-time quantitative PCR and the 2(T)(-Delta Delta C) method. *Methods* **25**, 402–408 (2001).

Author contributions

Additional information

How to cite this article: Wang, J., Wang, L., Li, X. & Mao, C. Virus activated artificial ECM induces the osteoblastic differentiation of mesenchymal stem cells without osteogenic supplements. *Sci. Rep.* **3**, 1242; DOI:10.1038/srep01242 (2013).